Structure
Short Article
CellPress

Coordinated Rearrangements between Cytoplasmic and Periplasmic Domains of the Membrane Protein Complex ExbB-ExbD of *Escherichia coli*

Aleksandr Sverzhinsky,[1] Lucien Fabre,[2] Andrew L. Cottreau,[1] Damien M.P. Biot-Pelletier,[1] Sofia Khalil,[1,5] Mihnea Bostina,[3,6] Isabelle Rouiller,[2] and James W. Coulton[1,4,*]
[1]Department of Microbiology and Immunology, McGill University, Montreal, QC H3A 2B4, Canada
[2]Department of Anatomy and Cell Biology, McGill University, Montreal, QC H3A 2B4, Canada
[3]Facility for Electron Microscope Research, McGill University, Montreal, QC H3A 2B4, Canada
[4]Microbiome and Disease Tolerance Centre, McGill University, Montreal, QC H3A 2B4, Canada
[5]Present address: Department of Biochemistry, Faculty of Science, Alexandria University, Alexandria 21526, Egypt
[6]Present address: Otago Centre for Electron Microscopy, Department of Microbiology and Immunology, University of Otago, Dunedin 9016, New Zealand
*Correspondence: james.coulton@mcgill.ca
http://dx.doi.org/10.1016/j.str.2014.02.010

SUMMARY

Gram-negative bacteria rely on the ExbB-ExbD-TonB system for the import of essential nutrients. Despite decades of research, the stoichiometry, subunit organization, and mechanism of action of the membrane proteins of the Ton system remain unclear. We copurified ExbB with ExbD as an ~240 kDa protein-detergent complex, measured by light scattering and by native gels. Quantitative Coomassie staining revealed a stoichiometry of $ExbB_4$-$ExbD_2$. Negative stain electron microscopy and 2D analysis showed particles of ~10 nm diameter in multiple structural states. Nanogold labeling identified the position of the ExbD periplasmic domain. Random conical tilt was used to reconstruct the particles in three structural states followed by sorting of the single particles and refinement of each state. The different states are interpreted by coordinated structural rearrangements between the cytoplasmic domain and the periplasmic domain, concordant with in vivo predictions.

INTRODUCTION

The cell envelope of Gram-negative bacteria consists of two bimolecular leaflets, the cytoplasmic membrane (CM) and outer membrane (OM), separated by the compartment termed periplasm. For transport of larger essential nutrients such as ferric siderophores or vitamin B_{12} across the OM, bacteria rely on TonB-dependent transporters (Noinaj et al., 2010). These receptors bind their substrates with high affinity and ensure transport by contacting the Ton system, an energy transduction complex that is embedded within the CM. Given the absence of both ATP-hydrolyzing proteins and a proton gradient across the OM, no source of energy exists at that membrane (Braun, 2006). Energy is therefore derived from the chemiosmotic gradient maintained across the CM. TonB, in complex with ExbB and ExbD, transduces this energy, effecting conformational rearrangements at the periplasmic face of OM receptors and thereby facilitating passage of nutrients into the periplasm (Nikaido, 2003).

ExbB and ExbD function by coupling TonB to the proton gradient across the CM (Braun et al., 1996; Larsen et al., 1999). Mutations in genes encoding ExbB and ExbD resulted in a 90% loss of TonB-dependent activity (Ahmer et al., 1995), with residual activity attributed to homologs TolQ and TolR proteins (Braun and Herrmann, 1993). ExbB and ExbD also display high homology to flagellar motor proteins MotA and MotB; they may share similar mechanisms for transduction of chemiosmotic energy (Zhai et al., 2003). ExbB stabilizes and copurifies with ExbD, suggesting the two proteins exist in complex (Braun et al., 1996; Fischer et al., 1989; Held and Postle, 2002). Furthermore, these two proteins displayed crosslinked adducts upon addition of formaldehyde (Ollis et al., 2009).

For ExbB topology, three transmembrane (TM) helices were proposed (Kampfenkel and Braun, 1993; Karlsson et al., 1993) and were redefined (Baker and Postle, 2013) using a recently published consensus algorithm. The first two helices are separated by a large cytoplasmic loop. ExbB could be crosslinked in vivo into dimers and tetramers (Higgs et al., 1998). The cytoplasmic carboxy termini of monomer ExbBs may facilitate this oligomerization through protein-protein contacts (Jana et al., 2011). Tetrameric complexes appear to be the predominant oligomer and to be composed of two ExbB dimers (Jana et al., 2011). ExbD displays topology similar to TonB, having one predicted TM helix embedded within the CM and the majority of its residues including the C terminus within the periplasm (Kampfenkel and Braun, 1992). Through in vivo formaldehyde crosslinking experiments, ExbD was shown to form homodimers as well as heterodimers with TonB (Ollis et al., 2009). The ExbD residues immediately following the TM domain provide conformational flexibility (Ollis et al., 2012).

While the quaternary structure of the TonB-ExbB-ExbD complex remains unknown, estimates of stoichiometry based on per cell copy numbers indicated a TonB:ExbB:ExbD ratio of 1:7:2 (Higgs et al., 2002). Recent analyses (Pramanik et al.,

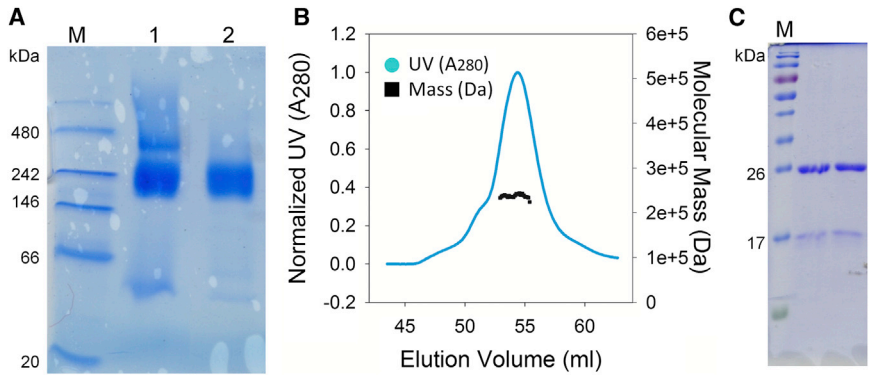

Figure 1. Molecular Mass and Protein Content of the Principal Protein-Detergent Complex

(A) BN-PAGE of ExbB-ExbD-His_6 post-IMAC (lane 1) and post-SEC (lane 2). The principal PDC migrated to ~242 kDa.

(B) ExbB-ExbD-His_6, purified by IMAC and preparative SEC, was assayed by SEC-MALLS. Light scattering measured the principal PDC at ~237 ± 5 kDa.

(C) SDS-PAGE and Coomassie staining of consecutive monodisperse fractions from preparative SEC.

M indicates molecular mass markers.

See also Figures S1, S2, and S7.

2011) of complex stoichiometry used laser-induced liquid bead ion desorption mass spectrometry on detergent-solubilized complexes of ExbB-ExbD. At moderate desorption laser energies, the oligomeric state of ExbB was reported to be mainly hexameric ($ExbB_6$) with minor amounts of trimeric ($ExbB_3$), dimeric ($ExbB_2$), and monomeric oligomers. Under the same conditions, ExbB-ExbD formed a subcomplex, reported as mostly $ExbB_6$-ExbD.

To further explore the structural organization of this membrane protein complex, 3D reconstruction of purified ExbB-ExbD in multiple conformations is reported, calculated by single particle electron microscopy (EM). Our data demonstrate potential coordinated rearrangements between the cytoplasmic and the periplasmic domains of the particles.

RESULTS

Purification and Biochemical Characterization of ExbB-ExbD-His_6

Escherichia coli cells containing pExbBD were grown, induced and extracted with 1% n-dodecyl-β-D-maltopyranoside (DDM). Protein-detergent complexes (PDCs) were subjected to immobilized metal ion affinity chromatography (IMAC), capturing the His_6-tag that was engineered at the C terminus of ExbD. The eluate was analyzed by SDS-PAGE followed by silver staining (Figure S1A available online), identifying only two prominent bands at 26 kDa and 17 kDa, and by western blotting (Figure S1B) disclosing a single band at 17 kDa and demonstrating that ExbD is His_6-tagged and that ExbB coeluted. The bands were excised, trypsinized, and submitted for mass spectrometry (MS) using LC-MS/MS. The proteins were identified as ExbB and ExbD, respectively (Figure S1C).

Additional analyses provided indication of multiple complexes formed between ExbB and ExbD-His_6. Following retention (150 kDa molecular weight cut-off [MWCO]) and concentration of IMAC-eluted material, analytical size exclusion chromatography (SEC) demonstrated a prominent peak with a shoulder indicative of higher molecular weight species (Figure S2; post-IMAC). SDS-PAGE gel and Coomassie staining confirmed that all complexes are composed of ExbB and ExbD in apparently different proportions. The principal ExbB-ExbD-His_6 complex was obtained by preparative SEC and showed apparent monodispersity by analytical SEC (Figure S2; post-SEC); comparison of its elution volume to calibrated standards of soluble proteins identified a Stokes radius (R_{st}) of 60–62 Å.

Analysis of Protein-Detergent Complexes: ExbB-ExbD in DDM

Blue-native PAGE (BN-PAGE) analysis of post-IMAC and post-SEC PDCs found the principal complex to be ~242 kDa (Figure 1A). The post-IMAC PDCs were analyzed by multiangle laser light scattering coupled to the preparative SEC column (SEC-MALLS). Experimental values for molecular mass of the principal PDC by light scattering were 237 ± 5 kDa (Figure 1B). Quantitative Coomassie staining of the protein constituents separated by SDS-PAGE revealed a molar ratio of 2 ExbB:1 ExbD-His_6 (Figure 1C). In the context of an ~240 kDa PDC, such a molar ratio can only be extrapolated to four ExbB molecules and two ExbD molecules ($ExbB_4$-$ExbD_2$-His_6) calculated to 138.6 kDa plus ~100 kDa DDM.

Single Particle Electron Microscopy of ExbB-ExbD-His_6

2D Imaging

Initial observations of $ExbB_4$-$ExbD_2$-His_6 by negative staining with uranyl formate showed homogeneous distribution of particles ~10 nm in diameter and present in various orientations on the EM grid (Figure 2A). From ~32,000 selected images of single particles, ~28,000 were validated with the SPARX program Iterative Stable Alignment and Clustering (ISAC) by reproducibly clustering into stable classes (Yang et al., 2012). From the analysis of the 449 resulting classes, a predominant density across the center of the particles was observed (Figure 2B, red bracket). Two density extensions were commonly seen below the central density (Figure 2B, green arrowheads); a third density extension was observed in some of the particles (Figure 2B, pink arrowhead). The latter density, when observed, occupies varying positions with respect to the central density (Figure 2C, top row). The two densities that are almost always seen in the ISAC classes also show slight differences in position (Figure 2C, bottom row). These analyses demonstrated multiple structural states and even continua of some positions of the $ExbB_4$-$ExbD_2$ complex, thus precluding generation of initial models by the common-line algorithm and subsequent refinement.

Considering that an $ExbB_4$-$ExbD_2$-His_6 complex would contain 14 TM domains (12 TM of ExbB and 2 TM of ExbD) and ~100 kDa DDM, the large central density (4 × 10 nm) is proposed to be the TM region of the PDC (Figure 2B, red

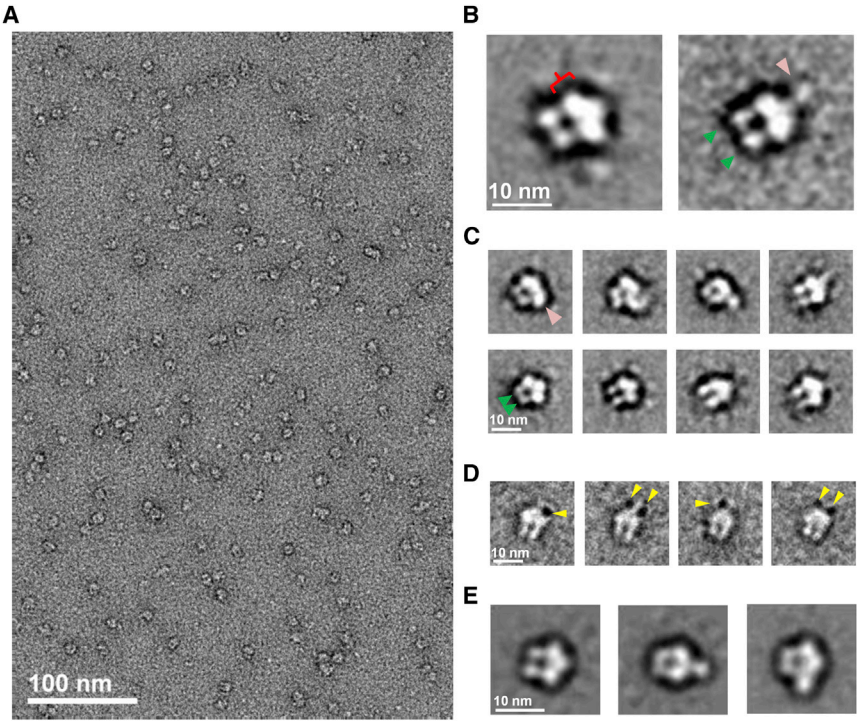

Figure 2. ExbB-ExbD-His$_6$ Particles

(A) Uranyl formate negative staining identified particles of ~10 nm diameter.

(B) Particles were classified using ISAC; two of the characteristic classes are shown. Classes share a common density (red bracket). Two densities on one side of the central density (green arrowheads) and some of the particles contain a single density on the other side of the central density (pink arrowhead).

(C) A gallery of ISAC classes showing structural variability in the densities above (top row, pink arrowhead) and below (bottom row, green arrowheads) the central density.

(D) Ni-NTA-Nanogold labeling of ExbB-ExbD-His$_6$ clustered with K means (20 seeds) reveals the C terminus (periplasmic domain) of ExbD (yellow arrowheads).

(E) The three class averages of untilted RCT particles used to reconstruct 3D models.

Classes shown in (B) and (C) contain between 23–93 particles (average 72 particles), classes in (D) contain 8–10 particles, and classes in (E) contain 459–604 particles.

See also Figures S3 and S7.

bracket). Recognizing that ExbD's C terminus (~12 kDa) is localized in the periplasm, we wished to orient the periplasmic and cytoplasmic sides of the TM region. After labeling ExbD's His$_6$ tag with Ni-NTA-conjugated 1.8 nm Nanogold particles, the gold label was consistently observed either in contact with the single density or localized to that position even if the single density was not observed (Figure 2D, yellow arrowheads). Furthermore, there were often two Ni-NTA-Nanogold particles associated with that side of the TM region. This identifies the periplasmic side (Figure 2B, pink arrowhead); the flexible density would therefore be the complex's periplasmic domains, almost exclusively composed of ExbD. Densities below the TM region would consequently be the cytoplasmic domain (Figure 2B, green arrowheads), with little contribution from ExbD and most contribution from ExbB's cytoplasmic loop and its C terminus.

3D Reconstructions

3D classification of the single particles required reliable references. The random conical tilt (RCT) approach was used to reconstruct reference models using tilted images. Three class averages of 2D images (Figure 2E) represented the three major states of the ISAC classes based on ExbD's periplasmic position: undefined, extended, or membrane-parallel. Although the resultant 3D volumes were flattened, they clearly showed the periplasmic domain in various positions with some having positional differences in the cytoplasmic portion (Figures S3A–S3C). These reference models were used to sort the untilted particles according to the position of ExbD's periplasmic domain (see 3D Refinement in the Supplemental Experimental Procedures). The models were used as multireferences in Xmipp's maximum-likelihood 3D classification (ML3D) (Scheres et al., 2007). The three resultant in-class data sets were then used to refine their respective RCT reference model using ML3D refinement, thereby improving (no longer flattened) the reference models (Figures S3A′, S3B′, and S3C′). To gain precision in the sorting of particles, the updated models were used as multireferences for a second round of ML3D classification of the entire data set, resulting in 18,812, 3,255, and 5,562 particles for the ExbD-undefined, ExbD-extended, and ExbD-membrane-parallel classes, respectively.

In-class conformational variability was investigated using unbiased seeds (Scheres et al., 2007). Only the ExbD-undefined class (68% of particles) showed substantial differences in the cytoplasmic portions (Figure S4). The cytoplasmic densities formed a ring below the ovoid micellar head. The conformational difference within this class is the arrangement of these densities. As expected, no density was observed on the periplasmic side of the micellar heads. The model with the greatest number of particles was chosen as the representative ExbD-undefined map for projection matching angular refinement.

Following projection matching angular refinement using their respective data sets, Figure 3 displays 3D EM maps for the representative ExbD-undefined (Figure 3A), the ExbD-extended (Figure 3B), and the ExbD-membrane-parallel states (Figure 3C). The volumes of the two ExbD-defined maps were set to ~240 kDa using a partial specific volume of 1.21 Å^3/Da (Harpaz et al., 1994). The ExbD-extended and ExbD-membrane-parallel maps have resolutions of 27 Å and 24 Å, respectively, according to the Fourier Shell Correlation (FSC) cut-off of 0.5 (Rosenthal and Henderson, 2003) and show complete Euler angle distributions (Figure S5). The 3D EM maps are consistent with the class averages and single particles (Figure S6).

Considering that the ExbD-undefined map (7,322 particles) does not account for electron potential of ~25 kDa (two ExbD

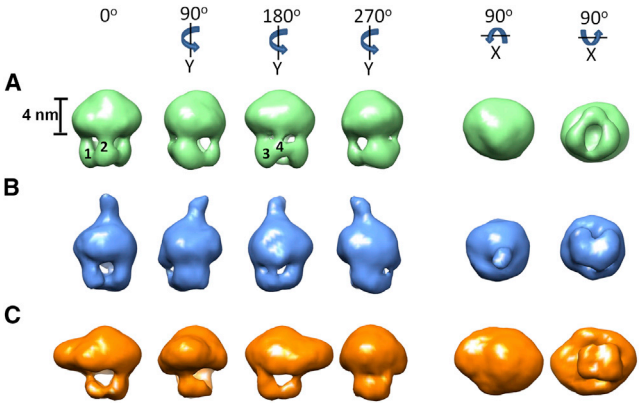

Figure 3. 3D EM Maps of Three Structural States of ExbB-ExbD-His$_6$
All rotations are relative to 0°. A 4 nm scale bar is inserted to propose the membrane boundary.
(A) Refined reconstruction of the ExbB-ExbD-His$_6$ complex in the ExbD-undefined state shows four densities (labeled) extending from the TM region forming a ring when viewed from the cytoplasmic face. No density above the TM domain was observable by EM. The cytoplasmic domain shows 2-fold symmetry despite the lack of symmetry imposed during reconstruction.
(B) Refined reconstruction of the ExbD-extended state shows two thick densities below the TM region. They form a compact arrangement viewed from the cytoplasmic face.
(C) Refined reconstruction of the ExbD-membrane-parallel state also has two thick extensions forming a compact arrangement on the cytoplasmic side of the membrane protein complex. The periplasmic density lies along the TM region in this state.
See also Figures S3–S6.

periplasmic domains), its volume was set to ~215 kDa. Its resolution was 21 Å according to the 0.5 FSC criterion and it too shows complete Euler angle distribution. The 3D EM map shows four extensions descending from the TM region, plausibly the ExbB cytoplasmic domains (Figure 3A). No symmetry was imposed during the reconstruction process. The final map displays apparent 2-fold symmetry in the cytoplasmic domains, except that one of the four extensions has less electron potential than the others. The ExbD-extended class (12% of particles) and ExbD-membrane-parallel class (20% of particles) share the same micellar head as the ExbD-undefined class, but show no conformational variability in the cytoplasmic portion. Instead of forming a ring, the two thick extensions join at the distal end, forming a compact arrangement (Figures 3B and 3C). An interpretation is that two ExbB molecules would be in close proximity to form the two thicker extensions seen in the two ExbD-defined reconstructions. This interpretation suggests a link between the periplasmic domain of ExbD and the cytoplasmic arrangement of ExbB.

DISCUSSION

Elucidating the structural basis of energy transduction across the periplasm of *E. coli* led us to adopt electron microscopy that identifies oligomers formed by ExbB-ExbD. Despite many years of studies, the stoichiometry, subunit organization and mechanism of action remain unclear. Here, we show that following solubilization in DDM, ExbB copurified by IMAC with ExbD-His$_6$. While free from any other coeluting proteins, the post-IMAC ExbB-ExbD-His$_6$ complexes were present in apparently multiple stoichiometries. Analytical SEC identified a major peak (corresponding to a R_{st} of 60 Å–62 Å) among minor peaks of greater radius. However, because SEC cannot be used to measure molecular weights, we used two well-established techniques employing independent criteria. The principal PDC measured ~240 kDa by BN-PAGE (migrating to the same distance as B-phycoerythrin) and by SEC-MALLS.

Monodispersity of the principal PDC was achieved with a preparative SEC column followed by quantitative Coomassie staining to identify a molar ratio of 2 ExbB:1 ExbD-His$_6$. An ExbB$_4$-ExbD$_2$-His$_6$ complex (calculated as 138.6 kDa) is consistent with the above measurements of protein content in the PDC. ExbB and ExbD-His$_6$ have similar arginine, lysine, and histidine content (25 and 22 residues, respectively), a prerequisite for stoichiometric Coomassie binding and quantitation (Tal et al., 1985). Other preparative SEC fractions contained solely ExbB and ExbD-His$_6$ but in different proportions. They were detected as the leading shoulder in the post-IMAC SEC (Figure S2), as the upper band in BN-PAGE (Figure 1A, lane 1) and as a range of particle sizes in electron micrographs (Figure S7A). It is possible that ExbB and ExbD form multiple oligomers in vivo as a mechanism for sequestration of subunits in nonactive form. Indeed, such a scenario could explain previous in vivo quantitation experiments that found ExbB to outnumber ExbD 7:1 despite their transcription from the same operon (Higgs et al., 2002). The possibility that complex formation is induced by the His$_6$ tag was ruled out by experiments where we cleaved the tag and still observed similar elution profiles by analytical SEC (data not shown). Although an in vitro functional assay remains to be established, a stoichiometry of ExbB$_4$-ExbD$_2$ is consistent with in vivo cysteine scanning mutagenesis studies (Jana et al., 2011) that found ExbB to form predominantly tetramers at chromosomal levels of expression. Their mutant strains displayed essentially wild-type behavior in phenotypic assays. In similar experiments, ExbD was found to form homodimers when its periplasmic residues were individually substituted by cysteine, even in the absence of ExbB (Ollis and Postle, 2011). All substitutions were active in iron transport under nonreducing conditions. Taken together, we obtained monodisperse PDCs of an ExbB$_4$-ExbD$_2$ complex, a physiologically relevant stoichiometry and therefore amenable to structural analyses.

We next turned to single particle EM to elucidate the PDC's subunit organization in DDM. We found that the ~10 nm particles all shared a common 4 × 10 nm central density that we identified as the TM region, consistent with previous direct measurements of cytoplasmic membranes (Mitra et al., 2004). The PDCs would be composed of 14 TM domains and ~100 kDa of DDM and/or lipids. 3D-EM reconstruction often begins with an ab initio model generated from 2D class averages and subsequent refinement using single particles. This strategy failed to produce a single solution for the ExbB$_4$-ExbD$_2$-His$_6$ complex when starting from different numbers of class averages and using the common line algorithm to produce models. While the complex is biochemically homogeneous, it is structurally variable. Although not observable in the majority of particles, one-third of them contain a domain that was experimentally identified by Ni-NTA-Nanogold as ExbD-His$_6$'s periplasmic domain. Two

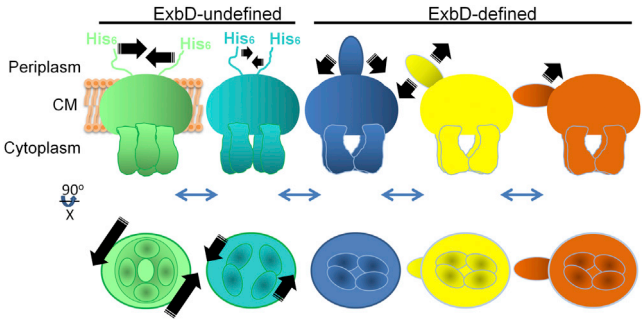

Figure 4. Schematic Representations of ExbB-ExbD-His$_6$ Show Coordinated Rearrangements between Cytoplasmic and Periplasmic Domains

Two "disordered" ExbD-His$_6$ periplasmic domains were added where the Ni-NTA-Nanogold was observed. The transition from the ExbD-undefined state to the ExbD-defined state is correlated with a rearrangement of the ExbB cytoplasmic domains. In the ExbD-undefined state, the ExbB cytoplasmic domains remain mostly as separated densities, forming a ring below the TM region. Formation of a dimerized periplasmic domain is correlated with the four thin densities becoming two thick densities, tightly interacting below the TM region. Once the periplasmic domains are dimerized, they are seen as flexible, moving as a unit.

Nanogold particles were sometimes seen in this position (Figure 2D), even when the periplasmic domain was not observed. Yet, this domain was observed more frequently in the labeling experiments, suggesting that the presence of Ni-NTA can coordinate two His$_6$ tags together. When this domain is observable by EM (~25 kDa together), we interpret this to represent two ExbD-His$_6$ periplasmic domains in close proximity. When this domain is not observed as in the majority of particles, they are therefore not ordered.

To distinguish different conformations of the ExbB$_4$-ExbD$_2$-His$_6$ complex, we used the method of RCT to produce an initial model of the ExbD-undefined particles and two models of the ExbD-defined particles in two structural states. In the first of two steps to assess structural variability, we focused on the ExbD periplasmic domain. First, using ML3D, the entire data set was sorted based on similarity to the three RCT references. ML3D refinement was chosen to improve the reference models so that they could be used again to sort the entire data set with more precision. Second, each ExbD-specific structural state reference model could then be used to gauge structural variability within its own data set by the use of unbiased seeds. The two ExbD-defined data sets showed no further structural discrepancy. Instead, they shared a similar arrangement of their cytoplasmic domains: two thick extensions from the TM region joining at the distal end. The ExbD-extended and ExbD-membrane-parallel models were refined to 27 Å and 24 Å, respectively. In contrast, the ExbD-undefined data set contained subsets of particles with varying arrangements of the cytoplasmic domains, but they universally formed a ring below the TM region. The differences between the subsets lay in the number, thickness and arrangement of the cytoplasmic domains, suggesting some dynamic in this part of the complex. Refinement of the representative ExbD-undefined model resulted in a 21 Å map showing apparent 2-fold symmetry of the four cytoplasmic domains.

The multitude of arrangements in the cytoplasmic domains of the ExbD-undefined data set (Figure S4) and the two ExbD-defined maps (Figures 3B and 3C) mirror in vivo findings of closely interacting ExbB C termini (Jana et al., 2011). Those authors report that cysteine-substituted ExbB mutants spontaneously form disulfide crosslinks even in the reducing environment of the cytoplasm. Furthermore, they found that crosslinked ExbB tetramers became ExbB dimers upon heating, thereby suggesting that ExbB exists in vivo as a dimer of dimers. We show that the ExbB-ExbD-His$_6$ cytoplasmic portion has four domains with 2-fold symmetry (ExbD-undefined) that can rearrange into two thicker domains (ExbD-defined). Another study substituting ExbB TM domain residues with alanine found that the TM domains are substantially involved in multimeric assembly (Baker and Postle, 2013), consistent with our observations of no gross rearrangements of the TM region between the maps. Baker and Postle (2013) also found evidence that two of ExbB's TM domains participate in signal transduction between the cytoplasm and periplasm.

Figure 4 depicts an interpretation, using our EM models, where the transition of ExbB's cytoplasmic domains from a 2-fold symmetrical tetramer to a dimer is correlated with a dimerization of the ExbD periplasmic domains (green → blue). Our schematic diagram of ExbD-His$_6$ dimerization also shows the periplasmic domains in dynamic positions with respect to the TM region, moving as a unit (blue → orange). This is supported by in vivo crosslinking studies that identified many ExbD periplasmic residues contributing to its homodimerization and its heterodimerization with TonB (Ollis and Postle, 2011). These authors measured increased formation of homodimers in the absence of TonB and suggested a functional role for dimerized ExbD. Furthermore, they claim that the periplasmic domains dimerized only after dynamically adopting many conformations, consistent with our data that two-thirds of the particles had no observable ExbD-His$_6$ periplasmic domain and yet were labeled by Nanogold. Ollis et al. (2012) hypothesized that this flexibility may be physiologically related to coupling signals from TM domains to periplasm. The authors found that the ~20 residues immediately following the TM domain position the ExbD periplasmic domain for contact with TonB's periplasmic domain, thereby allowing TonB to become energized for its interaction with OM receptors.

We show an oligomeric arrangement of an ExbB-ExbD complex captured in multiple structural states. The interpretation of our structures is consistent with in vivo stoichiometric data and predictions of subunit interactions and flexibility. Our medium-resolution 3D structures shed light on subunit organization and their rearrangements as a mechanism of communication between cytoplasm and periplasm. These results form the basis of future studies elucidating TonB's structural role in complex with ExbB and ExbD.

EXPERIMENTAL PROCEDURES

Details of the experimental procedures are found in the Supplemental Experimental Procedures. Briefly, the ExbB-ExbD complex was obtained from a single fraction following preparative SEC and prepared for EM by negative staining with uranyl formate. Two image batches were recorded: (1) 50 micrographs leading to ~16,000 particles, and (2) 50 image pairs using the RCT approach at tilt angles of 0° and −60° leading to ~16,000 particle pairs.

Particles were extracted (128 × 128 pixel images) and normalized. Untilted particles were combined and analyzed by ISAC over 16 generations, validating 449 classes as stable and reproducible, accounting for ~28,000 particles. Additional stable ISAC classes are shown in Figure S7B.

SEC-purified ExbB-ExbD-His_6 was incubated with 1.8 nm Ni-NTA-Nanogold (Nanoprobes) for 10 min at 1:1 (v/v) followed by dilution in SEC running buffer and concentration in a 150 kDa MWCO concentrator. The retentate was imaged by EM and classes were generated using K means clustering.

Untilted particles from the RCT image pair data set were classified using K means clustering followed by maximum-likelihood 2D classification. 3D reconstructions were independently calculated for 32 classes with the particle images from the tilted images using back-projection (Figures S7C–S7E show examples of tilt pairs). The ISAC-validated untilted particles were sorted based on similarity to three of the RCT reconstructions and then used to refine the models. The final volumes have been deposited into the EMDB: ExbD-undefined (EMD-5901), ExbD-extended (EMD-5902), and ExbD-membrane-parallel (EMD-5903).

ACCESSION NUMBERS

The Electron Microscopy Data Bank (EMDB) accession numbers for the data reported in this paper are EMD-5901, EMD-5902, and EMD-5903.

SUPPLEMENTAL INFORMATION

Supplemental Information includes Supplemental Experimental Procedures and seven figures and can be found with this article online at http://dx.doi.org/10.1016/j.str.2014.02.010.

ACKNOWLEDGMENTS

This work was supported by operating grants to J.W.C. from the Canadian Institutes of Health Research (CIHR reference number 200709MOP-178048-BMA-CFAA-11449) and I.R. (CIHR reference number 86693MOP). I.R. is a CIHR New Investigator. The Groupe d'étude des protéines membranaires (GÉPROM), supported by the Fonds de la recherche en santé du Québec (FRSQ), awarded a Projet Novateur to both principal investigators. A.S. was awarded fellowships from the CREATE program, Cellular Dynamics of Macromolecular Complexes, Natural Sciences and Research Engineering Council (NSERC) of Canada; GÉPROM; and the F.C. Harrison and the Rozanis Funds, Department of Microbiology and Immunology, McGill University. L.F. and A.L.C. were awarded fellowships from GÉPROM. D.B.-P. received a PGS-M scholarship from NSERC and an international training award from FRSQ. Canada Foundation for Innovation provided infrastructure for the Facility for Electron Microscope Research, McGill University (http://www.medicine.mcgill.ca/femr/home.html). Mass spectrometry services were provided by Marcos Di Falco, Genome Quebec Proteomics Platform. This work was facilitated by computing resources from CLUMEQ under Compute/Calcul Canada. We appreciate laboratory support from Nathalie Croteau and suggestions on the manuscript by B. Cousineau, J.M. Kollman, and J. Kashul. This paper is dedicated to Professor R.G.E. Murray, electron microscopist, who celebrates his 70th year of graduation (1943) from McGill University.

Received: December 13, 2013
Revised: February 5, 2014
Accepted: February 11, 2014
Published: March 20, 2014

REFERENCES

Ahmer, B.M., Thomas, M.G., Larsen, R.A., and Postle, K. (1995). Characterization of the *exbBD* operon of *Escherichia coli* and the role of ExbB and ExbD in TonB function and stability. J. Bacteriol. *177*, 4742–4747.

Baker, K.R., and Postle, K. (2013). Mutations in *Escherichia coli* ExbB transmembrane domains identify scaffolding and signal transduction functions and exclude participation in a proton pathway. J. Bacteriol. *195*, 2898–2911.

Braun, V. (2006). Energy transfer between biological membranes. ACS Chem. Biol. *1*, 352–354.

Braun, V., and Herrmann, C. (1993). Evolutionary relationship of uptake systems for biopolymers in *Escherichia coli*: cross-complementation between the TonB-ExbB-ExbD and the TolA-TolQ-TolR proteins. Mol. Microbiol. *8*, 261–268.

Braun, V., Gaisser, S., Herrmann, C., Kampfenkel, K., Killmann, H., and Traub, I. (1996). Energy-coupled transport across the outer membrane of *Escherichia coli*: ExbB binds ExbD and TonB *in vitro*, and leucine 132 in the periplasmic region and aspartate 25 in the transmembrane region are important for ExbD activity. J. Bacteriol. *178*, 2836–2845.

Fischer, E., Günter, K., and Braun, V. (1989). Involvement of ExbB and TonB in transport across the outer membrane of *Escherichia coli*: phenotypic complementation of *exb* mutants by overexpressed *tonB* and physical stabilization of TonB by ExbB. J. Bacteriol. *171*, 5127–5134.

Harpaz, Y., Gerstein, M., and Chothia, C. (1994). Volume changes on protein folding. Structure *2*, 641–649.

Held, K.G., and Postle, K. (2002). ExbB and ExbD do not function independently in TonB-dependent energy transduction. J. Bacteriol. *184*, 5170–5173.

Higgs, P.I., Myers, P.S., and Postle, K. (1998). Interactions in the TonB-dependent energy transduction complex: ExbB and ExbD form homomultimers. J. Bacteriol. *180*, 6031–6038.

Higgs, P.I., Larsen, R.A., and Postle, K. (2002). Quantification of known components of the *Escherichia coli* TonB energy transduction system: TonB, ExbB, ExbD and FepA. Mol. Microbiol. *44*, 271–281.

Jana, B., Manning, M., and Postle, K. (2011). Mutations in the ExbB cytoplasmic carboxy terminus prevent energy-dependent interaction between the TonB and ExbD periplasmic domains. J. Bacteriol. *193*, 5649–5657.

Kampfenkel, K., and Braun, V. (1992). Membrane topology of the *Escherichia coli* ExbD protein. J. Bacteriol. *174*, 5485–5487.

Kampfenkel, K., and Braun, V. (1993). Topology of the ExbB protein in the cytoplasmic membrane of *Escherichia coli*. J. Biol. Chem. *268*, 6050–6057.

Karlsson, M., Hannavy, K., and Higgins, C.F. (1993). ExbB acts as a chaperone-like protein to stabilize TonB in the cytoplasm. Mol. Microbiol. *8*, 389–396.

Larsen, R.A., Thomas, M.G., and Postle, K. (1999). Protonmotive force, ExbB and ligand-bound FepA drive conformational changes in TonB. Mol. Microbiol. *31*, 1809–1824.

Mitra, K., Ubarretxena-Belandia, I., Taguchi, T., Warren, G., and Engelman, D.M. (2004). Modulation of the bilayer thickness of exocytic pathway membranes by membrane proteins rather than cholesterol. Proc. Natl. Acad. Sci. USA *101*, 4083–4088.

Nikaido, H. (2003). Molecular basis of bacterial outer membrane permeability revisited. Microbiol. Mol. Biol. Rev. *67*, 593–656.

Noinaj, N., Guillier, M., Barnard, T.J., and Buchanan, S.K. (2010). TonB-dependent transporters: regulation, structure, and function. Annu. Rev. Microbiol. *64*, 43–60.

Ollis, A.A., and Postle, K. (2011). The same periplasmic ExbD residues mediate *in vivo* interactions between ExbD homodimers and ExbD-TonB heterodimers. J. Bacteriol. *193*, 6852–6863.

Ollis, A.A., Manning, M., Held, K.G., and Postle, K. (2009). Cytoplasmic membrane protonmotive force energizes periplasmic interactions between ExbD and TonB. Mol. Microbiol. *73*, 466–481.

Ollis, A.A., Kumar, A., and Postle, K. (2012). The ExbD periplasmic domain contains distinct functional regions for two stages in TonB energization. J. Bacteriol. *194*, 3069–3077.

Pramanik, A., Hauf, W., Hoffmann, J., Cernescu, M., Brutschy, B., and Braun, V. (2011). Oligomeric structure of ExbB and ExbB-ExbD isolated from *Escherichia coli* as revealed by LILBID mass spectrometry. Biochemistry *50*, 8950–8956.

Rosenthal, P.B., and Henderson, R. (2003). Optimal determination of particle orientation, absolute hand, and contrast loss in single-particle electron cryomicroscopy. J. Mol. Biol. *333*, 721–745.

Scheres, S.H.W., Gao, H., Valle, M., Herman, G.T., Eggermont, P.P., Frank, J.C., and Carazo, J.M. (2007). Disentangling conformational states of macromolecules in 3D-EM through likelihood optimization. Nat. Methods *4*, 27–29.

Tal, M., Silberstein, A., and Nusser, E. (1985). Why does Coomassie Brilliant Blue R interact differently with different proteins? A partial answer. J. Biol. Chem. *260*, 9976–9980.

Yang, Z., Fang, J., Chittuluru, J., Asturias, F.J., and Penczek, P.A. (2012). Iterative stable alignment and clustering of 2D transmission electron microscope images. Structure *20*, 237–247.

Zhai, Y.F., Heijne, W., and Saier, M.H. (2003). Molecular modeling of the bacterial outer membrane receptor energizer, ExbBD/TonB, based on homology with the flagellar motor, MotAB. Biochim. Biophys. Acta *1614*, 201–210.